ARTICLE

Forme fruste keratoconus detection with OCT corneal topography using artificial intelligence algorithms

Eugénie Mourgues, MD, Virgile Saunier, MD, David Smadja, MD, David Touboul, MD, PhD, Valentine Saunier, MD

Purpose: To differentiate a normal cornea from a forme fruste keratoconus (FFKC) with the swept-source optical coherence tomography (SS-OCT) topography CASIA 2 using machine learning artificial intelligence algorithms.

Setting: Monocentric, performed in CHU Bordeaux, Bordeaux, France.

Design: Retrospective case–control.

Methods: 3 groups were included: KC group (108 eyes), FFKC (88 eyes), and normal corneas (162 eyes). The data were analyzed and processed using the Dataiku data science platform. Machine learning models (random forest [RF], logistic regression [LR]) were used to develop a multiclass classifier for automated early KC detection. The models were trained using a training database and tested using a test database. Then, algorithms were compared with the Ectasia Screening Index (ESI), which is an OCT-topography inherent screening score for ectasia.

Results: The LR and RF detected FFKC with an area under the curve of 0.99 and 0.98, respectively. The sensitivities of LR (100%) and RF (84%) were better than the ESI (28%) for the diagnosis of FFKC. However, ESI has a maximum specificity (100%) compared with the LR (100%) and 90% for RF.

Conclusions: This study identified discriminating topographic parameters to be considered in refractive surgery screening on SS-OCT CASIA 2. An algorithm capable of classifying normal eyes vs FFKC cases was developed, with improved performance compared with the ESI score.

J Cataract Refract Surg 2024; 50:1247–1253 Copyright © 2024 Published by Wolters Kluwer on behalf of ASCRS and ESCRS

Keratoconus (KC) is a progressive degenerative disease affecting young patients in whom the cornea assumes a conical shape because of progressive stromal thinning.[1] The significant visual impact induced by myopia and irregular astigmatism degrades the quality of life in these patients.[2]

The surge in laser vision correction has prompted the need for a sensitive detection system to identify early signs of KC, reducing the risk of postlaser in situ keratomileusis (LASIK) ectasia, notably since Seiler et al. highlighted this risk.[3,4]

Although the incidence of post-LASIK ectasia is very low, ranging from 0.033% to 0.6%, it is one of the most feared complications.[5,6]

There is a lack of unified criteria to define subclinical KC and forme fruste KC (FFKC). According to Henriquez et al., the most common subclinical KC definition used refers to an eye with topographic signs of KC and/or suspicious topographic findings under normal slitlamp examination and KC in the fellow eye, and the most common FFKC definition refers to an eye with normal topography, normal slitlamp examination, and KC in the fellow eye.[7] The Randleman team recently named this entity "unaffected asymmetric KC eye (AKC)" when the topography is strictly normal (and visual acuity corrected to 20/20) in one eye and the other eye presents with frank KC.[8]

Multiple detection scores have been developed to assist in the diagnosis of KC and FFKC, including the Belin Ambrioso Enhanced Display or BAD-D on the Pentacam (Oculus Optikgeräte GmbH), which is the most widespread, the suspect corneas decision tree for the Galilei G4 (Ziemer Ophthalmic Systems AG) or the Score Analyzer on the Orbscan (Bausch & Lomb, Inc.), and more recently the Score Analyzer on the Anterion (Heidelberg Engineering GmbH).[9–13] The Scheimpflug technology with a Placido disc is widely used; however, corneal tomography mapping generated from optical coherence tomography (OCT)

Submitted: February 25, 2024 | Final revision submitted: May 22, 2024 | Accepted: August 27, 2024

From the Ophthalmology Unit, University Hospital Bordeaux, Bordeaux, France (Mourgues, Saunier, Touboul, Valentine Saunier); Department of Ophthalmology, Hadassah Medical Center, Faculty of Medicine, Hebrew University of Jerusalem, Jerusalem, Israel (Smadja).

Corresponding author: Eugénie Mourgues, MD, Service d'ophtalmologie, CHU Bordeaux, Place Amelie Raba Leon, 33000 Bordeaux, France. Email: eugenie.mourgues@gmail.com.

0886-3350/$ - see frontmatter
https://doi.org/10.1097/j.jcrs.0000000000001542

imaging technology has emerged as a promising alternative owing to faster acquisition and less dependence on dry eyes and tear film condition.[14] Nevertheless, the literature is still poor in indicating the most relevant parameters and their cutoff values to be used for refractive surgery screening to identify corneas at risk of ectasia.[15]

The objective of this study was to propose high-performance artificial intelligence (AI)-based models to improve the current detection system for FFKC using the swept-source OCT (SS-OCT) topography CASIA 2 (Tomey Corp.).

METHODS

This single-center retrospective case–control study was conducted at the National Reference Center for Keratoconus at the University Hospital of Bordeaux, France.

The patients included in this study were seen in consultation as part of routine care between June 2020 and February 2023 and completed the unit's consent questionnaire, authorizing the use of data for research and anonymously. The study design was approved by the Research Ethics Committee of Bordeaux University and the hospital.

Population

Eighty-eight eyes from 88 patients were included in the FFKC group, 108 eyes from 56 patients in the KC group, and 162 eyes from 162 patients in the normal eye group. Demographic (age and sex) and topo-tomographic data were collected.

Inclusion and Exclusion Criteria

Three groups were included and analyzed.

Group KC Eyes affected by a confirmed bilateral KC were defined on the basis of elevation topography and confirmed by 2 expert physicians from the center (V.S., D.T.) according to the Rabinowitz criteria: corneal topography with an asymmetric bowtie pattern or localized steepening on the anterior or posterior surface, and at least one of the following slitlamp findings: stromal thinning, Fleischer ring greater than 2 mm arc, Vogt striae, and corneal scarring consistent with KC.[16,17] We used the topography from the SS-OCT CASIA 2 for the diagnosis. As KC is an asymmetrical pathology, both eyes of each patient were included (analyses section).

FFKC Group Eye with normal topography in a patient with proven contralateral KC or KC can be defined as unilateral. This definition corresponds to the AKC group defined by Hwang et al., and the same definition was used by Saad et al., which indicates no clinical evidence of disease, no physical findings on slitlamp examination, no definitive abnormalities on corneal imaging, and a corrected distance visual acuity of 20/20 or better.[8,13]

The topographies of this group were studied and validated by 2 experts from our center (V.S., D.T.). Some examples of FFKC included in this study are in the supplementary materials (Supplemental Figures 1–5, available at http://links.lww.com/JRS/B223).

Normal Group Normal eyes recruited from patients coming for a screening visit for refractive surgery, having undergone LASIK surgery without abnormal postoperative evolution for at least 1 year. For the study, preoperative topographies were used as part of the analysis (examples of FFKC topographies are in the Appendix). One eye was selected for each patient. Eyes were considered normal when no clinical signs of KC and no suggestive topographic patterns of suspected KC were found, such as asymmetric bowtie with skewed radial axes, focal or inferior steepening, central keratometry greater than 47.0 diopters, or corneas thinner than 480 μ m. The exclusion criteria for this group were previous ocular surgery, ocular pathology, familial history of KC, and contact lens wearing in the past week.

Patients with ocular pathologies other than KC or a history of eye surgery (other than LASIK in the normal group) were excluded. Poor fixation or examination quality also led to exclusion.

OCT Topography

Patients from all the 3 groups underwent topography using SS-OCT CASIA 2.[18] Measurements were performed using the SS-OCT topography of the anterior segment CASIA 2 (software v. 50.06) according to the manufacturer's guidelines, and measurements were taken by an experienced examiner. The OCT technology uses a fast-scanning light source that emits near-infrared light. A portion of the light reflected by the cornea is collected using a detector. Interferometry is used to measure the phase differences between the emitted and reflected lights. This generates interference, which is then analyzed to reconstruct a 3D image of the cornea.

The collected data were processed using dedicated software, which reconstructs a 3D image of the cornea. This image represents different layers of the cornea, including the anterior and posterior surfaces.

The infrared wavelength is 1310 nanometers, and the acquisition is rapid, taking only 0.3 seconds for a topography scan, with a scan rate of 50 000 scans-A per second. The axial resolution is less than 10 μm, and the transverse resolution is less than 30 μm.

The corneal topography data record were (1) keratometric and anterior surface elevation parameters, (2) keratometric and posterior surface elevation parameters, (3) pachymetry parameters, (4) Fourier decompositions and optical aberrations, and (5) Ectasia Screening Index (ESI) (Table 1).

Standard acquisition for topography was from an axial map. The keratometric parameters corresponded to a conventional TMS Standard Sagittal map. As with the conventional TMS, the paraxial calculation was performed using 1.3375 as the refractive index of the cornea.

Fourier series analysis decomposes any circumferential fluctuations of the corneal power into various components which have clinical correlates. The spherical component and regular astigmatism values are proportional to keratometric spherical and astigmatic powers. Asymmetry is a tilt of the cornea about the video–keratoscope axis. Irregular astigmatism reflects a series of optical imperfections that degrade retinal image quality. Fourier analysis can quantify irregular astigmatism as the sinusoidal variation in power.[19]

In the keratometric data, we collected the Instantaneous Posterior Index (IPI) which is a radius curvature map describing localized changes of the corneal shape and is converted to refractive power by the refractive index for conversion on the paraxial calculation.

Elevation maps were gathered for both the anterior and posterior surfaces of the cornea and indicate the difference obtained by subtracting the height of the reference sphere (Best fit sphere) from the height of the cornea. Elevation anterior highest (EAH) and elevation posterior highest (EPH) are the highest points.

ESI is a parameter derived from AI, provided by the SS-OCT CASIA 2, for which the formula and performance characteristics are unknown. ESI is an index used to detect ectasia patterns, such as KC, by analyzing and evaluating the anterior and posterior surfaces of the cornea. It assesses the presence of specific patterns indicative of ectasia. The interpretation rules are as follows: 0% to 4% indicates no ectasia pattern detected, 5% to 29% indicates a suspicious pattern of ectasia, and 30% or more indicates a corneal pattern compatible with ectasia. The specific composition of the parameters included in the ESI is not disclosed by the system. However, based on Figure 1, it can be inferred that parameters such as pachymetry, Fourier analysis, axial power keratometry, and instantaneous power posterior map are likely included in the algorithm.

Table 1. Description of parameters collected with the SS-OCT CASIA 2 and submitted to the AI algorithms

Curvatures	Fourier transform	Elevation settings	ESI	Pachymetry	Wavefront aberrations
Keratometry • Ksteep, Kflat, Kmean, axes Posterior index • Ksteep, Kflat, Kmean, axes Real • Ksteep, Kflat, Kmean, axes Axial map • Kmax 8 and 10 mm front • Kmax 8 and 10 mm posterior Tangential map • Ksteep 6 mm and x, y localization • IPI 6 mm and location x, y	Fourier index axial power • Keratometry ◦ Sphere, regular, asymmetry, high-order, axes (within 3 and 6 mm) • Anterior ◦ Sphere, regular, asymmetry, high-order, axes (within 3 and 6 mm) • Posterior ◦ Sphere, regular, asymmetry, high-order, axes (within 3 and 6 mm) • Real ◦ Sphere, regular, asymmetry, high-order, axes (within 3 and 6 mm) • Cylinder ◦ FK cylinder, FP cylinder, FR cylinder and their axes in 4, 5, and 6 mm	Anterior • EAH BFS • EAH in 3, 6, and 9 mm • And their location x, y Posterior • EPH BFS • EPH in the 3, 6 and 9 mm • And their location x, y Difference • EPH-EAH	Status • Score % • ESI anterior score % • ESI score posterior score %	Apex • Thinnest point and its location x, y	Anterior • Coma, coma axis, AS4, AS35, AS40, AS46, HOAs, Zernike S3, S4, S5, S6 within 4 and 6 mm Posterior • Coma, coma axis, AS4, AS35, AS40, AS46, HOAs, Zernike S3, S4, S5, S6 within 4 and 6 mm Total • Coma, coma axis, AS4, AS35, AS40, AS46, HOAs, Zernike S3, S4, S5, S6 within 4 and 6 mm

AI = artificial intelligence; AS3 = spherical aberration third order, same for the fourth, fifth, sixth order; AS35 = spherical aberration third order and fifth order; AS40 = spherical aberration Z_4^0; AS46 = spherical aberration fourth order and sixth order; BFS = best fit sphere; EAH = elevation anterior highest point; EPH = elevation posterior highest point; ESI = Ectasia Screening Index; FK = Fourier keratometry; FP = Fourier posterior; FR = Fourier real; HOAs = higher-order aberrations 3, 4, 5, and 6: It is the mean of the squares of the Zernike coefficients on orders 3, 4, 5, and 6 (RMS HOA); IPI = Instantaneous Posterior Index; K = keratometric

We were unable to include epithelial mapping data in our study because they were not accessible to the CASIA-2 software version in our department at the time of the study.

Use of AI Algorithms for Data Analysis

The main analysis was performed with the DATAIKU software using AI, in particular "machine learning." Two AI-based algorithms were tested in this study, logistic regression and random forest. The different algorithms are explained as follows:

Logistic Regression In logistic regression, we worked with 2 key components: the input vector X, which encapsulates various eye-related characteristics (N) gathered through data collection, and the target variable Y, which we aimed to predict. In our case, Y represented whether the eye is affected by KC or FFKC. The primary objective was to determine a function h that operates on input vector X (i.e., h(X)) and yields a value within the range of 0 to 1. This value signified the probability of a specific event occurring, such as the eye being affected by FFKC.

Function h was parameterized by N parameters, which must be fine-tuned to achieve the most accurate predictions. It is worth noting that the sigmoid function is a crucial component of the h function because it transforms the input vector into a probability, ensuring that its output always falls within the 0 to 1 range.[20]

Random Forest Random forest is a machine-learning technique that builds a robust model by combining forest trees. Each tree is constructed using a random subset of data through bootstrap resampling. The best variable for each split was chosen from a predefined set of randomly selected variables (in this study, 9 variables). Each tree contributed a "vote" to the final decision, and classification problems used the mode, while regression used the mean. The method also assesses variable importance to identify key features for prediction.

Random forest has advantages, such as modeling nonlinear class boundaries and providing variable importance. Importantly, it addresses the issue of overfitting common in machine learning models by building trees on different samples, enabling more efficient generalization and resilience to noisy or missing data.[21,22]

Algorithm Validation Method A cross-validation method was used with a fold-increase of 5. The cross-validation method consisted of dividing the data into 5 equal subsets, then training the model on 4 subsets and testing it on the fifth subset. This operation was repeated 5 times so that each subset was used once for the test and 4 times for the training.

Statistical Analyses

Metrics To assess robustness, we used metrics derived from the confusion matrix, which provides sensitivity and specificity (Supplemental Table 1, available at http://links.lww.com/JRS/B222). This matrix facilitated the comparison of an algorithm's predictions with actual values (true labels or classes) within a test dataset. We used recall (=sensitivity), specificity, and precision (=positive predictive value).

To provide a comprehensive assessment of the performance of our model, we used the F1 score, which combines both recall and precision into a single metric. In addition to these metrics, we also assessed the overall correctness of the model using accuracy, which is computed as the ratio of correct classifications to the total number of classifications: To visualize the trade-off between true positive and false positives, we used a receiver operating characteristic curve.

ESI Performance The interest of our work was to compare it with the performance of the ESI for detecting corneal ectasia. The sensitivity and specificity of the ESI score were calculated to assess its ability to detect FFKC within the study population.

We compared the sensitivity and specificity of the ESI calculated on our FFKC population with those of our logistic regression and random forest algorithm.

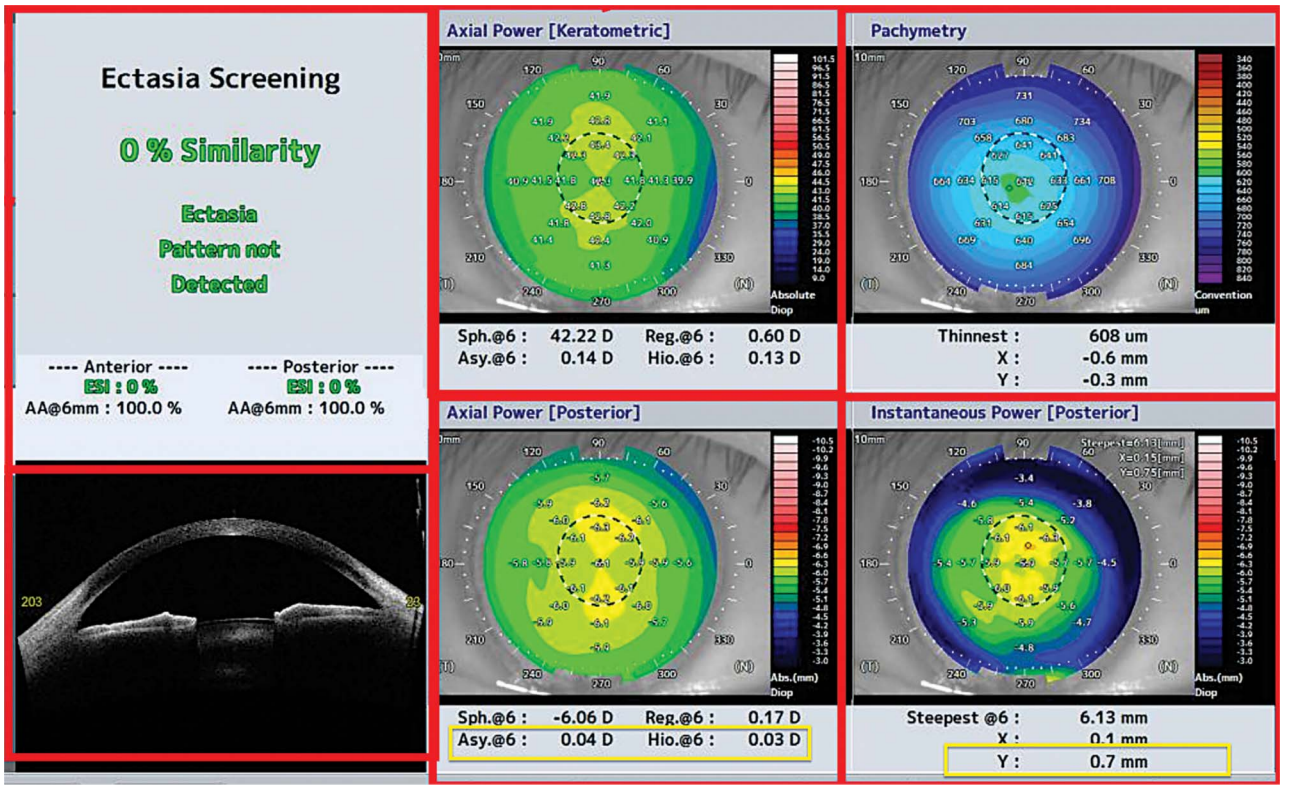

Figure 1. The yellow square shows the parameters used in logistic regression and random forest for the diagnosis of FFKC. FFKC = forme fruste keratoconus

RESULTS

Population Description

The demographic and topographical characteristics of the groups are presented in Supplemental Tables 2 and 3 (available at http://links.lww.com/JRS/B222). There were more men in the FFKC group (70% vs 30%, $P < .05$), and the patients were significantly younger (28 years vs 33, $P = .1$) than those in the normal eye group ($P < .05$). No significant differences in age or sex were observed between the KC and FFKC groups. There were no statistically significant differences in keratometric maximum (Kmax) and the keratometric flat (Kf) between the normal and FFKC groups.

Kmax is the maximum value of axial power (keratometric) within 10 mm area, and Kf is the flat meridian value. Corneal thinnest point (CTP) is the thinnest part of corneal thickness.

CTP was significantly lower in the FFKC group than in the normal group but remained above 500 μm in the FFKC group. All topographic parameters differed significantly between KC and FFKC groups.

AI Algorithms

In random forest and in logistic regression models, 205 variables were analyzed, and only the most discriminant ones were retained through automated relevance selection by the models, not by human intervention. Consequently, some data from CASIA 2 were not used for FFKC detection.

Detection of FFKC vs Normal The 2 algorithms performed well in detecting FFKC, as given in Table 2. The area under the receiver operating characteristic curve for detecting FFKC was 0.99 for logistic regression and 0.98 for the random forest (Supplemental Figures 6 and 7, available at http://links.lww.com/JRS/B223).

For logistic regression, the accuracy was 0.97, precision 0.93, recall 1, and F1 score 0.96.

For the random forest, the values were 0.94 and 1.0 for accuracy and precision, respectively. The recall was 0.84, and the F1 score was 0.91.

Logistic regression exhibited the highest diagnostic performances.

The most discriminating variables used by the random forest and logistic regression are the optical aberration parameters and Fourier transform data (Figure 2). In the random forest, we analyzed the decentering on the vertical axis (Y-axis) of different data such as IPIy, EPHy, and CTPy, and their importance factor in the algorithm ranged between 4% and 11% (Figure 2).

Table 2. Performances of the RF and the LR for detecting FFKC and normal eyes

Parameters	AUC ROC	Recall	Precision	F1 score	Accuracy
RF	0.977	0.84	1.0	0.91	0.94
LR	0.988	1.0	0.93	0.96	0.97

AUC = area under the curve; FFKC = forme fruste keratoconus; LR = logistic regression; RF = random forest; ROC = receiver operating characteristic

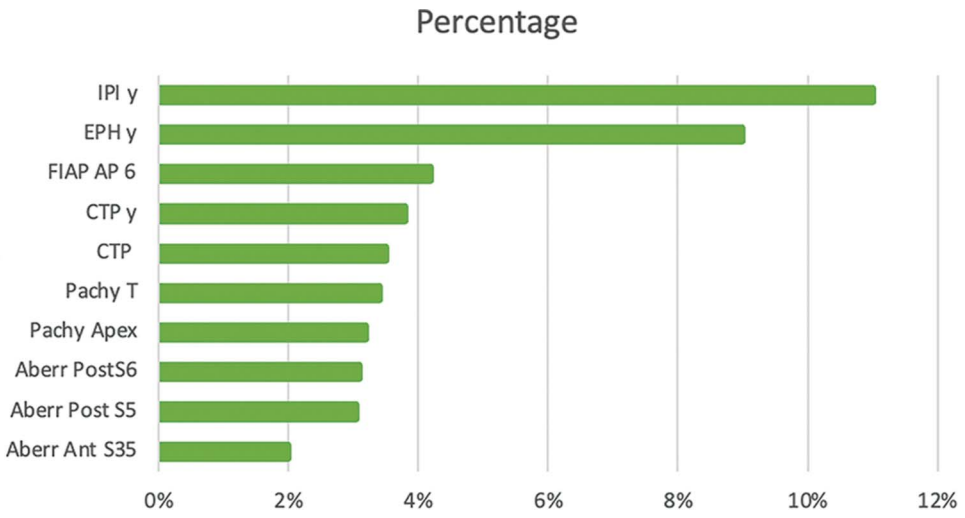

Figure 2. The histogram represents the data selected by the random forest algorithm and their importance in distinguishing FFKC from a healthy eye. The most discriminating data are grouped in this figure.Aberr Ant = aberration anterior; Aberr Post = aberration posterior; CTP = corneal thinnest point; EPHy = elevation posterior highest offset y in millimeters; FFKC = forme fruste keratoconus; FIAP AP 6 = Fourier index axial power asymmetry posterior within 6 mm; IPI Y = instantaneous posterior offset set Y in millimeters; Pachy T = pachymetry temporal

The confusion matrices of random forest and logistic regression for the diagnosis of FFKC are presented in Supplemental Tables 4 and 5, available at http://links.lww.com/JRS/B222, and the area under the curve also Supplemental Figures 6 and 7 (available at http://links.lww.com/JRS/B223).

Detection of KC vs Normal For the diagnosis of the KC vs normal eyes, the performance was excellent. The area under the receiver operating characteristic curve for KC detection was 1 for logistic regression and random forest. The accuracy, precision, F1 score, and recall were 1 for the random forest and logistic regression, respectively.

ESI Performance and Comparison With Our Algorithms This index considers 75% of corneas with FFKC as normal corneas, giving a specificity of 100% and sensitivity of 28% in our population (Table 3). By comparison, the sensitivity of the random forest is 84% and the specificity is 90%, the logistic regression had a better performance with 100% sensitivity and specificity (confusion matrix of random forest and logistic regression are given in Supplemental Tables 4 and 5, available at http://links.lww.com/JRS/B222, receiver operating characteristic curve for the ESI is depicted in Supplemental Figure 8, available at http://links.lww.com/JRS/B223).

DISCUSSION

OCT topography is increasingly emerging as a standard reference, and the research community requires scoring systems and algorithms that excel when applied to this technology.[23] The CASIA 2 OCT system offers a comprehensive set of 205 topographic parameters, which, however, cannot be thoroughly examined in the context of a refractive surgery screening consultation.

Table 3. Comparison of performances of the ESI, RF, and LR for diagnosis of FFKC

Parameters	Sensitivity (%)	Specificity (%)
ESI	28	100
LR	100	100
RF	84	90

ESI = Ectasia Screening Index; FFKC = forme fruste keratoconus; LR = logistic regression; RF = random forest

The CASIA algorithm, ESI, underperforms FFKC identification. It exhibited a sensitivity of only 28% and maintained specificity of 100%. Our developed algorithms have significantly improved detection sensitivity, as illustrated in Table 3, achieving up to 100% sensitivity in the case of logistic regression while preserving an identical specificity level.

Regardless of the algorithm used, it consistently excelled in identifying cases of KC without detection errors.

The performances of logistic regression and random forest for the detection of FFKC were similar to those in other studies.[24–26] The main difficulty in comparing these studies was the lack of a consensus definition for the FFKC and AKC groups.

The algorithm's parameter specifics provided valuable insights because the primary variables they rely on differ from typical clinical practice standards. Most of the differentiating parameters pertain to the posterior surface of the cornea. This observation was in line with the expected pathophysiology of both KC and FFKC.[27–29]

Less frequently used variables, such as Fourier transform asymmetry, off-center position of the CTP from the vertex, or data from the tangential map, assumed a significant role in random forest and logistic regression models.

Individually, each of these parameters demonstrated significance in the diagnosis of FFKC: Steinberg et al. also found that the Fourier transform asymmetry parameter was one of the most discriminating between normal eyes and the subclinical form of KC, with a validity of 0.81.[30] Their study was also performed on CASIA.

In addition, Kamiya et al. found that posterior elevation and posterior curvature showed the highest accuracy for single-map analysis; they used anterior-segment OCT CASIA and a neural network.[31]

The keratometric data are derived from the default axial map; however, it is possible to collect these values in tangential mode. As shown by Tummanapalli et al. and Rabinowitz, the tangential map is more sensitive than the axial map in detecting early KC.[32,33] Usually, this mode is dedicated to contactology,

but it seems that the minimal change in the decentering of the maximum posterior curvature is the first to be detected. The axial mode may smooth this change, and a tangential map should be considered for refractive surgery screening.

The robustness of our study emanated from the integration of a multitude of parameters with a deliberate emphasis on selecting the most critical ones.

Although CASIA provides the ESI, the algorithm underpinning it and the precise parameters used in its generation remain undisclosed. In the context of refractive surgery, attaining heightened sensitivity in detecting FFKC is paramount.

Furthermore, our study enrolled 88 FFKC cases, representing a sizable cohort. It can be inferred that ESI may not have been trained on a substantial number of FFKC, which could potentially diminish its sensitivity.

However, our sample size is a limitation, we have a comparatively large number of FFKC in comparison with previous studies, the overall patient count still falls short for AI algorithms, which are typically engineered to handle thousands of data entries.

Another limitation of our study is the absence of epithelial mapping. Most of our data were collected before we obtained the last update of the CASIA software, which not allowed us to obtain an epithelial map. It would be interesting to see if the mapping can discriminate FFKC, KC, and normal eyes, as it appears in the literature.[34,35]

The originality of this study lied in the utilization of the SS-OCT topography CASIA 2, which distinguished it from most other studies that used the Pentacam.[15,36–39] In 2018, the team lead by Yousefi was the first to develop an algorithm on the CASIA: AI permitted to diagnose and stage KC using a model based on unsupervised machine learning, this type of machine learning is designed to process smaller amounts of data.[40] The most significant difference from our study is the AI model; their algorithm is unsupervised. They used unsupervised density-based clustering in t-distributed stochastic neighbor embedding space to identify eyes with similar corneal features and to cluster eyes into objectively nonoverlapping groups. They showed that cluster III (mild KC) had a higher posterior ESI than anterior ESI, suggesting that posterior parameters were more discriminating. In addition, the extremity of cluster 2 (normal and FFKC groups) had an ESI not concordant with the unsupervised machine learning result, suggesting that some FFKCs are not diagnosed by ESI, as in our study.

There was a lack of AI studies on topographic OCT in the literature. Recently, the Saad team has developed an AI model for the detection of asymmetric KC using a model combining various parameters such as curvature, elevation, and pachymetric indices.[13] Their model was developed using Anterion OCT, and their findings closely align with ours, with an area under the curve of 0.954 compared with 0.99 for logistic regression in our study. Our study was one of the few conducted on CASIA 2 and the only 1 comparing the performance of ESI with another AI model. Topographers are not interchangeable, meaning that each algorithm is designed to be used by a specific type of topographer. Although the exact variables and their weightings used in calculating the ESI are not known, there are some similarities between the variables used in ours algorithms and those found in the ESI tab. Variables such as IPI and its location (X, Y), pachymetry map, and asymmetry of Fourier analysis are present in our random and logistic regression algorithms, indicating some overlap in the parameters considered for ectasia screening (Figures 1 and 2).

Using AI, we highlighted new parameters relevant to SS-OCT CASIA 2.

The random forest and logistic regression algorithms seem to be more efficient than the ESI; thus, changes to the variables included in the ESI may need to be considered by the manufacturer.

WHAT WAS KNOWN

- Artificial intelligence (AI) has emerged as a promising tool in the diagnosis of forme fruste keratoconus (FFKC) by enabling the integration of numerous corneal parameters and enhancing diagnostic accuracy.
- Most of the published studies have been conducted using Scheimpflug topographers; however, OCT technology is emerging as a replacement due to its enhanced performance capabilities.

WHAT THIS PAPER ADDS

- This study has led to the development of 2 high-performing AI algorithms for diagnostic of FFKC and KC using the CASIA 2, which can be used in routine clinical practice.
- Our diagnostic scores have demonstrated superior performance in diagnosing FFKC compared with those provided by the CASIA 2.

REFERENCES

1. Krachmer JH, Feder RS, Belin MW. Keratoconus and related noninflammatory corneal thinning disorders. Surv Ophthalmol. 1984;28(4):293–322. doi:10.1016/0039-6257(84)90094-8
2. Saunier V, Mercier AE, Gaboriau T, Malet F, Colin J, Fournié P, Malecaze F, Touboul D. Vision-related quality of life and dependency in French keratoconus patients: impact study. J Cataract Refract Surg. 2017;43(12):1582–1590. doi:10.1016/j.jcrs.2017.08.024
3. Tatar MG, Aylin Kantarci F, Yildirim A, Uslu H, Colak HN, Goker H, Gurler B. Risk factors in post-LASIK corneal ectasia. J Ophthalmol. 2014;2014:204191. doi:10.1155/2014/204191
4. Seiler T, Quurke AW. Iatrogenic keratectasia after LASIK in a case of forme fruste keratoconus. J Cataract Refract Surg. 1998;24(7):1007–1009. doi:10.1016/S0886-3350(98)80057-6
5. Sahay P, Bafna R, Reddy J, Vajpayee R, Sharma N. Complications of laser-assisted in situ keratomileusis. Indian J Ophthalmol. 2021;69(7):1658–1669. doi:10.4103/ijo.IJO_1872_20
6. Moshirfar M, Tukan AN, Bundogji N, Liu HY, McCabe SE, Ronquillo YC, Hoopes PC. Ectasia after corneal refractive surgery: a systematic review. Ophthalmol Ther. 2021;10(4):753–776. doi:10.1007/s40123-021-00383-w
7. Henriquez MA, Hadid M, Izquierdo L. A systematic review of subclinical keratoconus and forme fruste keratoconus. J Refract Surg. 2020;36(4):270–279. doi:10.3928/1081597X-20200212-03
8. Hwang ES, Perez-Straziota CE, Kim SW, Santhiago MR, Randleman JB. Distinguishing highly asymmetric keratoconus eyes using combined Scheimpflug and spectral-domain OCT analysis. Ophthalmology. 2018;125(12):1862–1871. doi:10.1016/j.ophtha.2018.06.020
9. Ambrósio R, Caiado ALC, Guerra FP, Louzada R, Sinha RA, Luz A, Dupps WJ, Belin MW. Novel pachymetric parameters based on corneal tomography for diagnosing keratoconus. J Refract Surg. 2011;27(10):753–758. doi:10.3928/1081597X-20110721-01

10. Ambrósio R, Faria-Correia F, Ramos I, Valbon BF, Lopes B, Jardim D, Luz A. Enhanced screening for ectasia susceptibility among refractive candidates: the role of corneal tomography and biomechanics. Curr Ophthalmol Rep. 2013;1(1):28–38. doi:10.1007/s40135-012-0003-z
11. Arce C. Qualitative and quantitative analysis of aspheric symmetry and Asymmetry on corneal surfaces. Poster Presented at ASCRS Annual Meeting, Boston, MA. Published online April 9, 2010
12. Saad A. Retrospective testing of the score for the detection of ectasia susceptibility: a case report of ectasia 7 years after LASIK. Int J Keratoconus Ectatic Corneal Dis. 2013;2(2):73–78. doi:10.5005/jp-journals-10025-1055
13. Saad A, Debellemanière G, Zeboulon P, Rizk M, Rouger H, Mazharian A, Grise-Dulac A, Panthier C, Gatinel D. Discrimination between keratoconus, forme fruste keratoconus and normal eyes using a novel OCT-based tomographer. J Cataract Refract Surg. 2023;49(11):1092–1097. doi:10.1097/j.jcrs.0000000000001275
14. Lin YY, Carrel H, Wang IJ, Lin PJ, Hu FR. Effect of tear film break-up on higher order aberrations of the anterior cornea in normal, dry, and post-LASIK eyes. J Refract Surg. 2005;21(5):S525–S529. doi:10.3928/1081-597X-20050901-21
15. Cao K, Verspoor K, Sahebjada S, Baird PN. Accuracy of machine learning assisted detection of keratoconus: a systematic review and meta-analysis. J Clin Med. 2022;11(3):478. doi:10.3390/jcm11030478
16. Rabinowitz YS. Keratoconus. Surv Ophthalmol. 1998;42(4):297–319. doi:10.1016/S0039-6257(97)00119-7
17. Rabinowitz YS, Yang H, Brickman Y, Akkina J, Riley C, Rotter JI, Elashoff J. Videokeratography database of normal human corneas. Br J Ophthalmol. 1996;80(7):610–616. doi:10.1136/bjo.80.7.610
18. MU-CASIA2-23032022_ENG.pdf
19. Sideroudi H, Labiris G, Georgantzoglou K, Ntonti P, Siganos C, Kozobolis V. Fourier analysis algorithm for the posterior corneal keratometric data: clinical usefulness in keratoconus. Ophthalmic Physiol Opt. 2017;37(4):460–466. doi:10.1111/opo.12386
20. Castro-Luna G, Pérez-Rueda A. A predictive model for early diagnosis of keratoconus. BMC Ophthalmol. 2020;20(1):263. doi:10.1186/s12886-020-01531-9
21. Lopes BT, Eliasy A, Ambrosio R. Artificial intelligence in corneal diagnosis: where are we? Curr Ophthalmol Rep. 2019;7(3):204–211. doi:10.1007/s40135-019-00218-9
22. Segal MR. Machine Learning Benchmarks and Random Forest Regression. Division of Biostatistics, University of California, San Francisco, CA. 2003. https://escholarship.org/uc/item/35x3v9t4. Accessed March 2024.
23. Chan TCY, Biswas S, Yu M, Jhanji V. Longitudinal evaluation of cornea with swept-source optical coherence tomography and Scheimpflug imaging before and after Lasik. Medicine (Baltimore). 2015;94(30):e1219. doi:10.1097/MD.0000000000001219
24. Golan O, Piccinini AL, Hwang ES, De Oca Gonzalez IM, Krauthammer M, Khandelwal SS, Smadja D, Randleman JB. Distinguishing highly asymmetric keratoconus eyes using dual Scheimpflug/Placido analysis. Am J Ophthalmol. 2019;201:46–53. doi:10.1016/j.ajo.2019.01.023
25. Lopes BT, Ramos IC, Salomão MQ, Guerra FP, Schallhorn SC, Schallhorn JM, Vinciguerra R, Vinciguerra P, Price FW Jr, Price MO, Reinstein DZ, Archer TJ, Belin MW, Machado AP, Ambrósio R Jr. Enhanced tomographic assessment to detect corneal ectasia based on artificial intelligence. Am J Ophthalmol. 2018;195:223–232. doi:10.1016/j.ajo.2018.08.005
26. Arbelaez MC, Versaci F, Vestri G, Barboni P, Savini G. Use of a support vector machine for keratoconus and subclinical keratoconus detection by topographic and tomographic data. Ophthalmology. 2012;119(11):2231–2238. doi:10.1016/j.ophtha.2012.06.005
27. Muftuoglu O, Ayar O, Ozulken K, Ozyol E, Akıncı A. Posterior corneal elevation and back difference corneal elevation in diagnosing forme fruste keratoconus in the fellow eyes of unilateral keratoconus patients. J Cataract Refract Surg. 2013;39(9):1348–1357. doi:10.1016/j.jcrs.2013.03.023
28. Itoi M, Kitazawa K, Yokota I, Wakimasu K, Cho Y, Nakamura Y, Hieda O, Teramukai S, Kinoshita S, Sotozono C. Anterior and posterior ratio of corneal surface areas: a novel index for detecting early stage keratoconus. PLoS One. 2020;15(4):e0231074. doi:10.1371/journal.pone.0231074
29. Elkitkat RS, Gharieb HM, Othman IS. Accuracy of the posterior corneal elevation values of Pentacam HR from different reference surfaces in early ectasia diagnosis. Int Ophthalmol. 2021;41(2):629–638. doi:10.1007/s10792-020-01618-8
30. Steinberg J, Casagrande MK, Frings A, Katz T, Druchkiv V, Richard G, Linke SJ. Screening for subclinical keratoconus using swept-source Fourier domain anterior segment optical coherence tomography. Cornea. 2015;34(11):1413–1419. doi:10.1097/ICO.0000000000000568
31. Kamiya K, Ayatsuka Y, Kato Y, Fujimura F, Takahashi M, Shoji N, Mori Y, Miyata K. Keratoconus detection using deep learning of colour-coded maps with anterior segment optical coherence tomography: a diagnostic accuracy study. BMJ Open. 2019;9(9):e031313. doi:10.1136/bmjopen-2019-031313
32. Tummanapalli SS, Potluri H, Vaddavalli PK, Sangwan VS. Efficacy of axial and tangential corneal topography maps in detecting subclinical keratoconus. J Cataract Refract Surg. 2015;41(10):2205–2214. doi:10.1016/j.jcrs.2015.10.041
33. Rabinowitz YS. Tangential vs sagittal videokeratographs in the "early" detection of keratoconus. Am J Ophthalmol. 1996;122(6):887–889. doi:10.1016/S0002-9394(14)70388-5
34. Reinstein DZ, Archer TJ, Gobbe M. Corneal epithelial thickness profile in the diagnosis of keratoconus. J Refract Surg. 2009;25(7):604–610. doi:10.3928/1081597X-20090610-06
36.–55. References 35–40 are listed in Supplemental Data File (http://links.lww.com/JRS/B221)

Disclosures: *None of the authors have any financial or proprietary interest in any material or method mentioned.*

First author:
Eugénie Mourgues, MD

Ophthalmology Unit, University Hospital Bordeaux, Bordeaux, France